Biomedical Signal Processing and Control 86 (2023) 105160

Contents lists available at ScienceDirect

Biomedical Signal Processing and Control

journal homepage: www.elsevier.com/locate/bspc

Subject-independent trajectory prediction using pre-movement EEG during grasp and lift task☆

Anant Jain [a], Lalan Kumar [a,b,c,*]

[a] Department of Electrical Engineering, Indian Institute of Technology Delhi, New Delhi 110016, India
[b] Bharti School of Telecommunication, Indian Institute of Technology Delhi, New Delhi 110016, India
[c] Yardi School of Artificial Intelligence, Indian Institute of Technology Delhi, New Delhi 110016, India

ARTICLE INFO

Keywords:
Brain–computer interface (BCI)
Electroencephalography (EEG)
Deep learning
Pre-movement
Inter-subject decoding
Subject-independent BCI

ABSTRACT

Electroencephalogram (EEG) based motor trajectory decoding for efficient control of brain–computer interface (BCI) systems has been an active area of research. The systems include prosthesis, rehabilitation and human-power augmenting devices. In this work, three-dimensional (3D) hand kinematics is estimated using pre-movement EEG signals during grasp and lift motion. Twelve subjects' data from the publicly available database WAY-EEG-GAL is utilized for this purpose. Multi-layer perceptron (MLP) and convolutional neural network-long short-term memory (CNN-LSTM) based deep learning frameworks are proposed that utilize the motor-neural information encoded in the EEG data preceding the actual movement execution. Frequency band features are analyzed for hand kinematics decoding using EEG data filtered in seven distinct ranges. The best performing frequency band features is taken for further analysis with different EEG window sizes and lag windows. Additionally, inter-subject hand trajectory decoding analysis is performed using leave-one-subject-out (LOSO) approach. The Pearson correlation coefficient along with hand trajectory are taken to evaluate decoding performance for the proposed neural decoders. This study explores the feasibility of inter-subject 3D hand trajectory decoding using EEG signals during reach and grasp task. The proposed CNN-LSTM decoder is able to achieve the grand correlation in three axes upto 0.730 and 0.627 in intra-subject and inter-subject settings, respectively, thus providing viable information regarding decoding hand position from pre-movement EEG signals for practical BCI applications.

1. Introduction

1.1. Background

Brain–computer interface (BCI) or brain–machine interface (BMI) utilizes brain activation for controlling external devices without embracing the peripheral nerves and muscles [1]. BCI is an emerging technology that demonstrate encouraging potential to ameliorate the quality of life for patients with motor impairments [2–4] and to interact with the healthy subjects [5,6]. With the advancement in neuroscience and machine learning algorithms, BCI systems have been utilized to assist, augment, or restore the brain's motor functionality [7]. The BCI system is confected of subsequent processes which commonly consist of neural signal acquisition, signal processing, feature extraction, human intention detection and user feedback signal generation. The neural activity can be recorded either by invasive or non-invasive recording systems. Although the invasive approach can result in more accurate and precise brain activity recognition, the sensors are surgically placed under the scalp for acquiring the neural signals [8,9]. However, non-invasive BCI utilizes neural activity by placing sensors over the scalp. Various non-invasive techniques utilized in BCI system include magnetoencephalography (MEG) [10], electroencephalogram (EEG) [11], functional near-infrared spectroscopy (fNIRS) [12,13] and functional magnetic resonance imaging (fMRI) [14,15].

EEG based BCI system has become popular because of high temporal resolution, portability and low-economy [16]. It has been utilized for various application such as emotion recognition [17,18], wearable exoskeleton [19–22], prosthesis [23–27], robot control [28]. It has been additionally utilized for motor imagery/execution classification for upper limb movement [29–32] and standing-sitting task [33]. EEG based BCI has been also employed to classify grasping movements [34], reach-and-grasp actions [35] and grasping objects [36,37]. Although classification based approach has been employed substantially, continuous kinematic estimation-based approach would yield enhanced

☆ This work was supported in part by DRDO - JATC project with project number RP04191G.
* Corresponding author.
E-mail addresses: anantjain@ee.iitd.ac.in (A. Jain), lkumar@ee.iitd.ac.in (L. Kumar).

https://doi.org/10.1016/j.bspc.2023.105160
Received 23 September 2022; Received in revised form 25 April 2023; Accepted 8 June 2023
Available online 20 June 2023

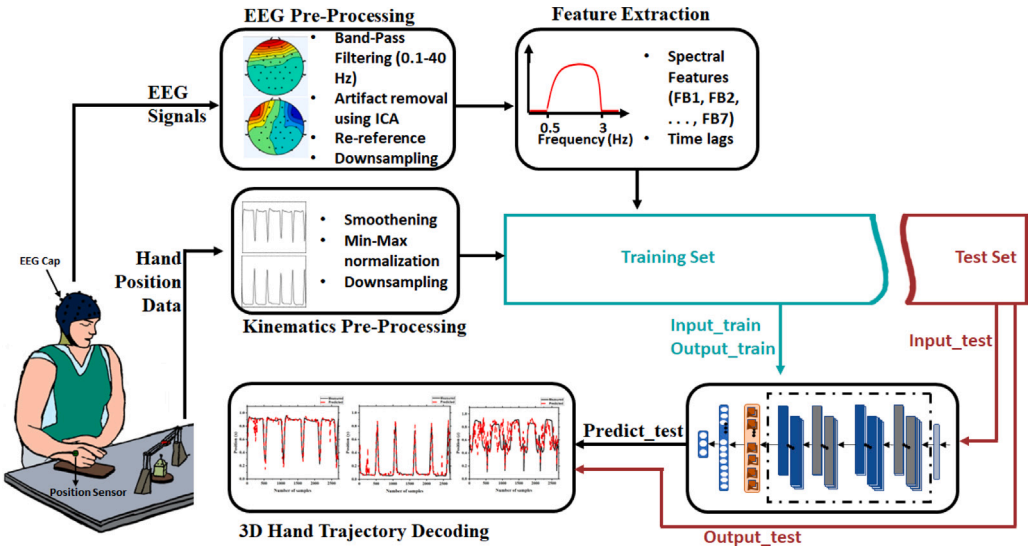

Fig. 1. Flowchart of proposed kinematics decoding framework for Grasp-and-Lift task.

performance and efficient control of assistive devices such as neural prosthesis, exosuit, or exoskeleton.

1.2. Related work

Multichannel EEG-based kinematics decoding for 2-D hand trajectory was investigated in [38] using multi-variable linear regression (mLR) neural decoder. A Kalman filter based mLR decoder was employed in particular for hand trajectory decoding with the reported mean correlation value of 0.60 ± 0.07 between the measured and predicted trajectory. Decoding of 3D hand trajectory using band-power EEG features and mLR as neural decoder was studied in [39]. Using scalp EEG signals, reconstruction of upper limb trajectories in 3D space was reported in [40] with mLR model as neural decoder. The mean Pearson's correlation coefficient between predicted and measured trajectories for hand, elbow and shoulder ranged in 0.24–0.49, 0.41–0.48 and 0.18–0.40, respectively. It is to be noted that mLR decoding technique is based on the linear relationship between input (EEG signals) and output variables (kinematics parameters). It is sensitive to data quality and outliers. The limitation of the mLR decoder can be overcome by utilizing the deep learning based decoding framework. Deep learning based decoders extract non-linear features from the input variables and are efficient to handle the outliers. Deep learning based neural decoders have been utilized in literature for kinematics parameter decoding [41–44] using scalp EEG signals. In [41], a deep learning architecture based on convolutional neural network - bidirectional long short-term memory (CNN-biLSTM) was utilized for arm trajectory decoding from EEG signals to control robotic arm. The mean correlation coefficient of 0.47 and 0.08 was reported therein for intra-subject and inter-subject, respectively. Hand motion was reconstructed for center-out movements using EEG and EMG signals in [42]. The predictor model was formed using mLR based EEG component and multi-layer perceptron (MLP) based EMG component for reconstruction of hand motion. The mean correlation value upto 0.753 was reported for the hand motion reconstruction. 3D hand trajectory was decoded for grasp and lift task using CNN-LSTM based neural decoder in [43]. Visual stimulus was considered as reference point therein for EEG signal. However, such visual stimulation limits the BCI system for day-to-day applications. A deep learning based neural decoder PreMovNet, that utilized movement-onset as reference point, was introduced in [44] for 3D hand trajectory estimation. The EEG data until movement-onset was utilized for hand kinematics estimation, thus not making it pre-movement in true sense.

1.3. Objectives and contributions

In this work, 3D hand kinematics is estimated using WAY-EEG-GAL dataset where EEG segment is chosen 50 ms to 350 ms prior to the movement, thus making it pre-movement in true sense. MLP and CNN-LSTM based deep learning frameworks are proposed for the trajectory decoding. The performance of the proposed decoding models are compared with state-of-the-art mLR model. As EEG signal has motion trajectory encoded approximately 300 ms before the actual movement, EEG data with various lags from movement-onset has been explored in this work. Frequency band analysis is performed first to find the optimum frequency band for decoding. The best performing frequency band features are taken for further analysis. The ablation study is performed for analyzing the significance of LSTM layer of the CNN-LSTM decoding model. Subject-independent capability of the decoding models have been explored to ensure the generalizability of the proposed trajectory prediction framework.

The organization of the article is as follows. The data acquisition and pre-processing steps are included in Section 2. The description related to frequency band features, neural decoders, training and evaluation of the decoding models is presented in Section 3. Performance evaluation for hand kinematics decoding is detailed in Section 4. Section 5 includes an extensive discussion of the results and Section 6 provides the conclusions about the research work.

2. Experimental setup

2.1. Data acquisition

In this analysis, open source WAY-EEG-GAL (Wearable interfaces for hAnd function recovery- EEG - grasp and lift) database [45] is utilized for hand kinematics decoding. 32-channel EEG recordings were collected in synchronization with hand movement at sampling frequency of 500 Hz as shown in Fig. 2(a). The kinematic data was obtained from a position sensor (P4) placed on the wrist of the participant. A sampling frequency of 500 Hz was utilized to record the kinematic data. The force and position sensors utilized in the experiment is shown in Fig. 2(b), with x-axis corresponding to lift force and z-axis to grip force. In particular, the database included recordings of twelve healthy subjects for right hand grasp and lift movement. In each trial, the subject's task to be executed was to reach and grasp a small object, lift it few centimeters up and hold it steady for a couple of seconds. The trial ended with replace and release the object to its original position,

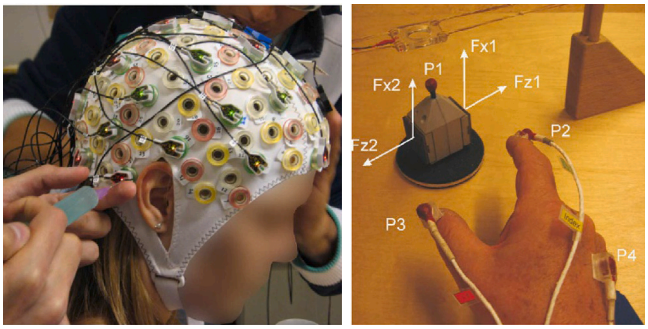

(a) (b)

Fig. 2. (a) 32-channel EEG acquisition system (b) Force and position sensors.

then bring the hand back to the resting position. The movement-onset to reach for grasping the object and putting it down was cued by an LED. Each participant executed 294 trials of grasp and lift task with variation in object's weight, contact surface, or both.

A LED mounted setup was put above the object, which could be switched on and off. Each trial commenced with turning on of the LED. The participant reached, grasped, lifted and held the object until the LED was activated. The LED was deactivated automatically after a couple of seconds, and then the participant put down and placed the object to its initial position. The trial ended with the participant bringing the arm back to its beginning position.

2.2. Data pre-processing

Scalp EEG data was initially band-pass filtered in the frequency range of 0.1–40 Hz using FIR filter to expunge baseline drifts. Re-referencing of EEG signals was performed using average re-referencing method. Further, eye movement artifacts and muscle artifacts were eradicated by utilizing the independent component analysis (ICA) technique. Denoised EEG data was downsampled to the sampling frequency of 100 Hz to reduce the computation cost. The EEG signals preprocessing was executed using the EEGLAB toolbox [46]. A total of 21 EEG channels were utilized from motor cortex region and occipital lobe for the neural decoding, namely F3, Fz, F4, FC5, FC1, FC2, FC6, C3, Cz, C4, CP5, CP1, CP2, CP6, P7, P3, Pz, P4, O1, Oz, and O2. Each of the EEG channel data was normalized using z-score normalization technique, given as

$$E^n[t] = \frac{e^n[t] - \mu_{e_n}}{\sigma_{e_n}} \tag{1}$$

where, $e^n[t]$ and $E^n[t]$ are the nth channel pre-processed and standardized voltage, respectively, at time t. The mean and standard deviation of e^n are denoted by μ_{e_n} and σ_{e_n}, respectively.

In order to remove kinematics measurement noise, low-pass filtering with cutoff frequency 2 Hz was performed. The frequency band 0–2 Hz is found to contain more than 99% of the raw kinematic data power [38,40]. Further, the min–max normalization was performed on the filtered kinematics data to scale it in range of $[0, 1]$ as,

$$P[t] = \frac{p[t] - p_{min}}{p_{max} - p_{min}} \tag{2}$$

where, $P[t]$ is normalized position coordinate value, $p[t]$ is measured position coordinate value, and $p_{min} - p_{max}$ are minimum-maximum position coordinates. The min–max normalization was performed for each position coordinate. Lastly, the normalized data was downsampled to 100 Hz.

3. Methodology

In this Section, the description of the EEG-based 3D hand kinematics decoding framework is presented. Fig. 1 illustrates the flow chart of the proposed hand kinematics decoding framework.

3.1. Frequency bands

The EEG frequency band (FB) was segregated into groups as FB1 (delta, 0.5–3 Hz), FB2 (theta, 4–8 Hz), FB3 (alpha, 9–12 Hz), FB4 (beta, 13–30 Hz), FB5 (gamma, > 30 Hz), FB6 (delta and theta, 0.5–8 Hz), and FB7 (delta, theta and alpha, 0.5–12 Hz). For hand kinematics decoding, the EEG data was filtered in each band group using a zero-phased 4th order Hamming-windowed FIR filter. All the selected 21 EEG channels were utilized for frequency band analysis. The filtered EEG data with appropriate delay (pre-movement) was utilized for the hand trajectory estimation. Three neural decoders: multi-linear regression (mLR), multi-layer perceptron (MLP) and CNN-LSTM model are utilized for hand kinematics decoding.

3.2. Data preparation

From each trial, the hand kinematics data was selected from the hand movement-onset until the participant put the hand back to its resting position. The movement-onset event corresponding to each trial was provided in the database. The cortical activation on the motor-cortex region was observed prior to the actual movement of the hand [43]. We assimilated the neural information corresponding to the motor activity by consolidating the EEG data prior to the hand movement. Various EEG lags and window sizes are explored for hand kinematics decoding. For example, EEG segment with lag of 50 ms and window size of 100 ms corresponds to −150 to −50 ms data, where 0 ms is at the movement-onset. For each kinematic segment, an input matrix of dimension $D \times (L * N)$ is generated where D, L, and N are data segment, size of time lag window and total selected EEG channels, respectively.

3.3. Multi-variable linear regression (mLR) model

Multi-variable linear regression (mLR) based kinematic decoding has been utilized for kinematics parameter estimation [38–40]. The mLR model utilizes multiple EEG inputs to decode hand position. The mLR model has input–output mapping given by:

$$mLR_x[t] = \alpha_x + \sum_{n=1}^{N} \sum_{l=l_1}^{l_2} \beta_x^{(nl)} E^n[t-l] \tag{3}$$

$$mLR_y[t] = \alpha_y + \sum_{n=1}^{N} \sum_{l=l_1}^{l_2} \beta_y^{(nl)} E^n[t-l] \tag{4}$$

$$mLR_z[t] = \alpha_z + \sum_{n=1}^{N} \sum_{l=l_1}^{l_2} \beta_z^{(nl)} E^n[t-l] \tag{5}$$

where, $mLR_x[t]$, $mLR_y[t]$, and $mLR_z[t]$ are the position of the hand in x, y, z-directions, respectively, at time t. $E^n[t-l]$ is the normalized EEG signal at time lag l. The number of time lags is in range from l_1 to l_2 with regression coefficients, α and β.

3.4. Multi-layer perceptron (MLP) model

The multi-layer perceptron (MLP) based neural decoder model consists a total of six layers. It includes batch normalization layer (B1), dense layers (D1, D2, D3 and D4), and output layer. D1, D2 and D3 consist of 128 neurons each, and D4 consists of 16 neurons. ReLU activation is utilized with each of the dense layer. The output layer consists of three neurons, each corresponding to the x, y, and z-directions of the hand position with input vector of size $L * N$. The model architecture of the MLP model is shown in Table 1.

Table 1
Model architecture of MLP model with 250 ms EEG time lag input.

MLP model	
Layer (type)	Output shape
Batch normalization (B1)	(None, 525)
Dense (D1)	(None, 128)
Dense (D2)	(None, 128)
Dense (D3)	(None, 128)
Dense (D4)	(None, 16)
Dense/output layer	(None, 3)

Table 2
Model architecture of CNN-LSTM model with 250 ms EEG time lag input.

CNN-LSTM model	
Layer (type)	Output shape
Batch Normalization	(None, 25, 21)
Conv1D (C1)	(None, 25, 256)
MaxPooling1D (M1)	(None, 5, 256)
Dropout	(None, 5, 256)
Conv1D (C2)	(None, 5, 128)
MaxPooling1D (M2)	(None, 1, 128)
LSTM	(None, 128)
Dense (D1)	(None, 128)
Dense(D2)/output layer	(None, 3)

3.5. CNN-LSTM model

In this Section, a CNN-LSTM based neural decoder is detailed for hand position decoding during grasp and lift task. The neural decoder comprises a total of nine layers including batch normalization layer, convolution layers (C_1 and C_2), max-pooling layers (M_1 and M_2), dropout layer, LSTM layer (L_1), and dense layers (D_1 and D_2). The C_1 and C_2 layers have a kernel size of 7 and 5 with 256 and 128 filters, respectively. Zero padding is also utilized for both C_1 and C_2 layers that results in same input and output size. ReLu activation unit is used in each convolution layer. Max-pooling layers, M_1 and M_2, have window size of 5 and 3, respectively. Dropout layer has a dropout rate of 0.25. LSTM layer, L_1, consists of 128 cells, along with the ReLU activation function. Dense layers, D_1 and D_2, have 128 and 3 neurons, respectively. Three neurons at the output layer yields the predicted hand position in the x, y, and z-directions. ReLU activation is used for convolution layers (C_1 and C_2), LSTM layer (L_1) and dense layers (D_1 and D_2). The input dimension to the model is $(L \times N)$ corresponding to 3D hand position output. The model architecture of the CNN-LSTM decoding model is shown in Table 2.

3.6. Training and evaluation

For training and performance evaluation of neural decoders, the data-set is divided into distinct training, validation, and test data. The training data is utilized for training the decoders, while the validation data is used for tuning model hyper-parameters and avoiding over-fitting of the decoders. The test data is utilized to evaluate performance of the trained neural decoders. The adaptive moment estimation (Adam) optimization algorithm [47] with loss function as mean squared error is adapted to train neural decoders based on deep learning architectures. The early stopping technique with patience of five epochs on validation data is utilized to avoid over-fitting of the decoding models. For subject-dependent analysis, a total of 294 trials are taken from each participant of the WAY-EEG-GAL data-set. The total trials for each participant are separated into three discrete subsets: (a) 234 trials data samples as training data; (b) 30 trials data samples as validation data; and (c) 30 trials data samples as test data.

For inter-subject analysis, the data from eleven participants is taken for training–validation and the total trials of remaining one participant are taken as testing data to evaluate the trained model. The inter-subject decoding analysis approach utilized is leave-one-subject-out (LOSO) technique. The training data is further divided into two subsets: (a) training subset and (b) validation subset. Training subset consists of 264 trials from each of eleven participants' data while the validation subset include remaining 30 trials from each of the selected eleven participants. Test set includes all 294 trials of the one left out subject to evaluate the decoding performance of the model. Pearson's correlation coefficient (PCC) between the predicted hand kinematics and measured kinematics data is taken as performance metric to evaluate the decoding performance of the neural decoders. The parameters of the decoding models are obtained by parameter optimization with different sets of parameters. The optimum performing parameters are selected for MLP and CNN-LSTM decoding models. In particular, the training step is computationally rigorous, while the estimation with trained model is brisk. Therefore, the trained decoding model can be utilized to control external devices such as exoskeletons/exosuits or prosthesis.

4. Performance evaluation

Pearson correlation coefficient (PCC) is considered as performance metric to evaluate the efficiency of the neural decoders for hand kinematics decoding. In particular, PCC is computed with various EEG window size. PCC is a linear correlation coefficient whose value ranges from −1 to +1. PCC value of −1, 0 and +1 represent a strong negative, zero and strong positive correlation, respectively. Pearson correlation coefficient between measured (P_x) and estimated (P_y) hand kinematic parameters with a total samples of T is defined as

$$\Pi(P_x, P_y) = \frac{1}{T-1}\sum_{i=1}^{T}\left(\frac{P_x^i - \mu^{P_x}}{\sigma^{P_x}}\right)\left(\frac{P_y^i - \mu^{P_y}}{\sigma^{P_y}}\right) \tag{6}$$

where, μ_q and σ_q are the mean and standard deviation of q, respectively, with $q \in \{P_x, P_y\}$.

Additionally, the hand trajectory estimation in x, y, and z-directions are plotted along with the measured trajectory for comparative analysis.

4.1. Intra-subject decoding analysis

4.1.1. Frequency band analysis

The 3D hand position trajectory decoding is performed on seven FBs (as detailed in Section 3.1) with EEG lags for twelve participants from WAY-EEG-GAL database. Three neural decoders are utilized for this purpose. Frequency band analysis is performed to find out the EEG frequency band that result in best trajectory decoding performance. The mean PCC values for distinct FBs and EEG time windows are presented in Table 3 for x, y and z-directions. In x and y-directions, the frequency band features in FB1 frequency band with 250 ms EEG window provides best PCC values for CNN-LSTM based neural decoder. However, in z-direction, CNN-LSTM based neural decoder with frequency band features in FB7 frequency band and EEG window of 350 ms gives best PCC value. It may be observed that MLP and CNN-LSTM based deep learning decoders perform significantly better than the traditional mLR neural decoder. The proposed neural decoder shows relatively low performance in z-direction. The noisy performance may be due to transitory hand movement in z-direction during the grasp and lift task. The best overall PCC (0.791, 0.799, and 0.600 for x, y, and z-directions) was achieved with CNN-LSTM model for EEG interval in −250 ms to 0 ms. Additionally, it may be observed that the performance of decoding models are significantly higher in lower frequency bands (FB1). Hence, FB1 frequency band is taken for further analysis.

Table 3
Frequency band analysis of neural decoders ((a) mLR, (b) MLP, and (c) CNN-LSTM) with EEG lag 0 ms and window size of 150 ms, 200 ms, 250 ms, 300 ms and 350 ms.

Frequency band	Direction	−150 to 0			−200 to 0			−250 to 0			−300 to 0			−350 to 0		
		(a)	(b)	(c)	(a)	(b)	(c)	(a)	(b)	(c)	(a)	(b)	(c)	(a)	(b)	(c)
FB1 (0.5–3 Hz)	x	0.507	0.734	0.764	0.497	0.731	0.762	0.501	0.753	**0.791**	0.501	0.750	0.771	0.505	0.761	0.771
	y	0.518	0.743	0.773	0.509	0.741	0.772	0.512	0.761	**0.799**	0.511	0.761	0.776	0.516	0.769	0.778
	z	0.381	0.578	0.557	0.375	0.591	0.582	0.383	0.606	0.600	0.372	0.616	0.598	0.367	0.621	0.619
FB2 (4–8 Hz)	x	0.021	0.631	0.625	0.033	0.647	0.654	0.045	0.646	0.646	0.069	0.626	0.639	0.089	0.624	0.636
	y	0.022	0.654	0.649	0.034	0.667	0.676	0.046	0.663	0.668	0.070	0.643	0.660	0.090	0.639	0.656
	z	0.025	0.412	0.375	0.034	0.418	0.382	0.047	0.415	0.377	0.063	0.423	0.377	0.078	0.423	0.400
FB3 (9–12 Hz)	x	0.137	0.500	0.493	0.239	0.496	0.498	0.283	0.518	0.524	0.333	0.502	0.499	0.365	0.503	0.515
	y	0.142	0.523	0.515	0.246	0.514	0.521	0.288	0.537	0.544	0.340	0.520	0.520	0.375	0.519	0.485
	z	0.094	0.427	0.417	0.172	0.414	0.396	0.207	0.403	0.394	0.213	0.396	0.367	0.216	0.394	0.364
FB4 (13–30 Hz)	x	0.129	0.399	0.403	0.194	0.423	0.444	0.227	0.427	0.465	0.257	0.435	0.489	0.278	0.431	0.511
	y	0.135	0.419	0.429	0.201	0.439	0.472	0.235	0.441	0.494	0.264	0.454	0.515	0.288	0.445	0.530
	z	0.081	0.376	0.413	0.123	0.375	0.442	0.143	0.375	0.442	0.153	0.376	0.433	0.162	0.367	0.430
FB5 (> 30 Hz)	x	0.090	0.275	0.296	0.106	0.295	0.327	0.123	0.274	0.352	0.152	0.234	0.349	0.178	0.263	0.371
	y	0.097	0.291	0.316	0.113	0.311	0.352	0.129	0.290	0.381	0.159	0.248	0.376	0.187	0.278	0.398
	z	0.076	0.229	0.262	0.090	0.253	0.276	0.101	0.220	0.278	0.117	0.189	0.266	0.129	0.196	0.269
FB6 (0.5–8 Hz)	x	0.460	0.720	0.740	0.460	0.727	0.754	0.466	0.748	0.768	0.469	0.744	0.775	0.476	0.744	0.766
	y	0.471	0.728	0.745	0.472	0.736	0.762	0.477	0.757	0.777	0.480	0.752	0.779	0.487	0.753	0.770
	z	0.350	0.571	0.570	0.355	0.586	0.589	0.351	0.611	0.602	0.344	0.606	0.608	0.343	0.622	0.616
FB7 (0.5–12 Hz)	x	0.432	0.715	0.723	0.436	0.721	0.744	0.442	0.727	0.766	0.452	0.738	0.752	0.461	0.730	0.753
	y	0.443	0.722	0.731	0.448	0.729	0.752	0.452	0.737	0.770	0.461	0.743	0.761	0.472	0.737	0.757
	z	0.332	0.589	0.594	0.335	0.603	0.618	0.334	0.608	0.627	0.329	0.613	0.630	0.329	0.619	**0.635**

Note: the bold entries represent the highest PCC value obtained using the neural decoders in x, y and z directions.

4.1.2. Trajectory analysis

In this Section, the predicted hand trajectory is compared herein with actual trajectory in x, *y* and *z*-directions. The measured and predicted hand trajectories in x, *y* and *z*-directions are plotted in Fig. 3(a)–(c) for mLR neural decoder, Fig. 3(d)–(f) for MLP model and Fig. 3(g)–(i) for CNN-LSTM model. The hand trajectories are plotted for participant 04 taking FB1 frequency band and EEG window of 200 ms. CNN-LSTM based deep learning neural decoders gives the lowest trajectory mismatch in all the three directions. The transient movement in *z*-direction leads to poor visual correlation.

4.1.3. Significance of LSTM layer

In this Section, ablation study of the CNN-LSTM decoding model is presented. In particular, the significance of LSTM layer in the proposed decoding model is analyzed. The decoding performance of the CNN-LSTM model is compared with a CNN-based model for this purpose. In this analysis, the LSTM layer of the proposed decoding model is omitted and all the model parameters remain same as CNN-LSTM model. The architecture of the CNN model is same as that in Table 2, replacing LSTM layer with GlobalMaxPooling1D layer. The analysis is performed for delta frequency band (FB1) with different EEG data windows. The performance of the proposed deep learning neural decoders is compared in Fig. 4 for all the three direction.

4.1.4. EEG lags analysis

Utilizing data up to movement onset does not make the model pre-movement in the true sense. It is to note that all the earlier analyses utilized EEG segment upto movement-onset. In this analysis, the hand movement trajectory is decoded using pre-movement EEG data with distinct window sizes and lags as shown in Table 4. EEG segment upto 250 ms prior to movement-onset is utilized. An increase in decoding accuracy can be observed with increase in window size of the EEG lags. The two deep learning based methods (CNN-LSTM and MLP) outperform the traditional mLR based approach. The two deep learning based methods perform almost similar. The best overall correlation achieved are 0.764, 0.771, and 0.623 in x, y, and *z*-directions, respectively for −350 ms to −50 ms EEG lag window using MLP decoder.

4.2. Inter-subject decoding analysis

Subject-independent hand trajectory decoding analysis is presented in this Section. Leave-one-subject-out (LOSO) approach is adopted to analyze inter-subject hand trajectory decoding during grasp and lift task. The decoding performance of each neural decoder and each test subject is given in Table 5 for different EEG window sizes. The mean PCC value of all the test subjects is calculated for each EEG window and direction to evaluate the performance of neural decoders. It is observed that decoding performance is improved with the increment of EEG window size. The deep learning based decoding models (CNN-LSTM and MLP) outperform mLR in decoding hand trajectory in all three directions. Decoding models with EEG window of 350 ms is optimal to decode 3D hand trajectory for grasp and lift task. The mean PCC values for CNN-LSTM decoding model with 350 ms EEG window are 0.690, 0.728, and 0.462 in x, y, and *z*-directions, respectively. This analysis shows that the deep learning based decoding models are able to learn subject-independent EEG features for hand trajectory decoding.

5. Discussion

The literature makes use of mLR decoding model for continuous kinematic estimation [38–40]. The Pearson's correlation coefficient between predicted and measured trajectories varies between 0.18–0.6 based on type of movement and body part involved. The detail is presented in Section 1.2. MLP and CNN-LSTM based deep learning models are utilized in this work for 3D hand trajectory decoding during grasp-and-lift task. Intra-subject and Inter-subject analysis is presented.

Frequency band analysis is presented first to find the optimum frequency band. Potential time series (PTS) data is utilized for this purpose. A detailed comparative analysis is presented for all the frequency bands and combinations. It may be noted from Table 3 that the delta band (FB1) gives best decoding performance in x and *y*-directions. FB7 frequency band outperforms slightly in *z*-direction when compared with FB1. The proposed PTS based deep learning neural decoders give decent decoding performance in theta, alpha and beta bands. It is

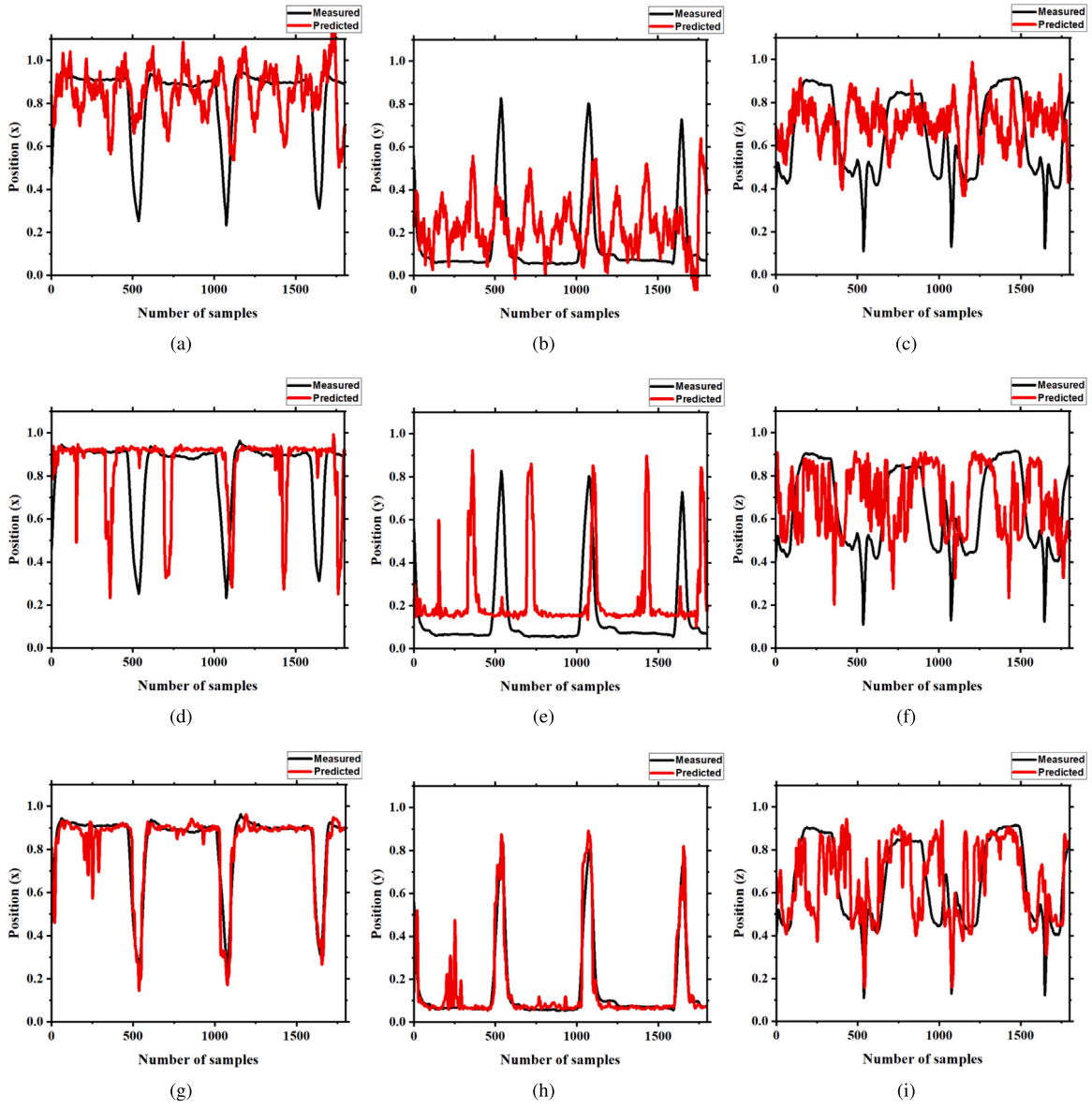

Fig. 3. Hand trajectory decoding in x, *y* and *z*-directions for participant-04 using mLR decoder in (a)–(c), MLP decoder in (d)–(f), and CNN-LSTM decoder in (g)–(i). −200 ms to 0 ms EEG window is taken in delta band.

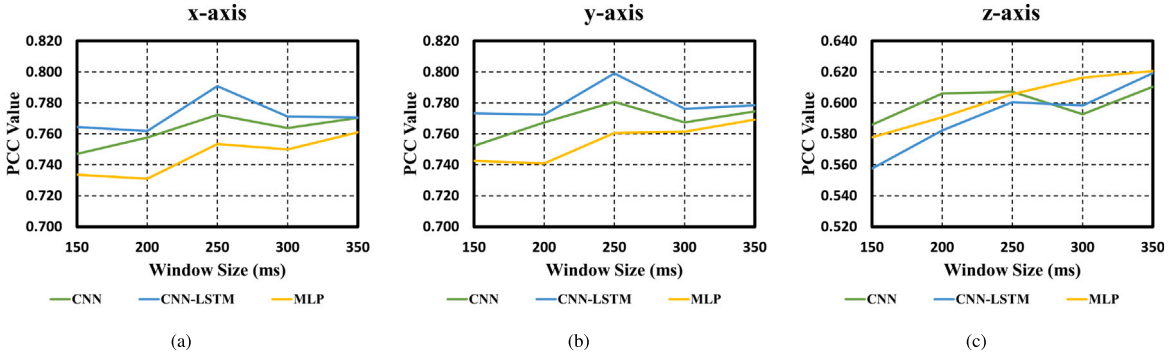

Fig. 4. Performance comparison of MLP, CNN and CNN-LSTM models in x, y, and *z*-directions with delta band EEG signals.

inline with the fact that low frequency (FB1) EEG signals have major contribution in decoding hand movements when utilizing PTS data [30,39,40,44,48,49]. Alpha, beta and low gamma bands have additionally been tried to decode 3D hand trajectory in [39]. Higher correlation is observed in these bands when bandpower time-series (BTS) is utilized. Hence, EEG signals in FB1 frequency band is considered for the further analysis. A higher correlation leads to better trajectory reconstruction as shown in Fig. 3.

Table 4
EEG lag analysis of neural decoders ((a) mLR, (b) MLP, and (c) CNN-LSTM) with various lag window and window sizes.

EEG lags		Decoders	x	y	z
Window size (ms)	Lag window (ms)				
100	−150 to −50	(a)	0.486	0.497	0.373
		(b)	0.735	0.745	0.578
		(c)	0.735	0.744	0.553
	−200 to −100	(a)	0.466	0.478	0.367
		(b)	0.729	0.737	0.585
		(c)	0.730	0.734	0.555
	−250 to −150	(a)	0.451	0.461	0.357
		(b)	0.742	0.751	0.582
		(c)	0.734	0.740	0.558
	−300 to −200	(a)	0.440	0.451	0.340
		(b)	0.726	0.734	0.579
		(c)	0.735	0.741	0.555
	−350 to −250	(a)	0.445	0.457	0.335
		(b)	0.732	0.741	0.581
		(c)	0.738	0.745	0.560
150	−200 to −50	(a)	0.489	0.501	0.375
		(b)	0.742	0.750	0.596
		(c)	0.732	0.741	0.558
	−250 to −100	(a)	0.475	0.485	0.364
		(b)	0.741	0.750	0.579
		(c)	0.735	0.742	0.548
	−300 to −150	(a)	0.464	0.475	0.348
		(b)	0.744	0.751	0.593
		(c)	0.741	0.744	0.554
	−350 to −200	(a)	0.468	0.480	0.342
		(b)	0.745	0.753	0.596
		(c)	0.737	0.741	0.560
200	−250 to −50	(a)	0.490	0.501	0.375
		(b)	0.751	0.761	0.599
		(c)	0.749	0.753	0.575
	−300 to −100	(a)	0.478	0.490	0.359
		(b)	0.745	0.753	0.604
		(c)	0.737	0.743	0.575
	−350 to −150	(a)	0.480	0.492	0.350
		(b)	0.751	0.760	0.607
		(c)	0.749	0.752	0.565
250	−300 to −50	(a)	0.490	0.501	0.367
		(b)	0.758	0.763	**0.625**
		(c)	0.747	0.754	0.568
	−350 to −100	(a)	0.489	0.500	0.354
		(b)	0.749	0.759	0.624
		(c)	0.737	0.742	0.570
300	−350 to −50	(a)	0.498	0.509	0.360
		(b)	**0.764**	**0.771**	0.623
		(c)	0.736	0.742	0.588

Note: the bold entries represent the highest PCC value obtained using the neural decoders in x, y and z directions.

Significance of LSTM layer in the proposed deep learning neural decoder is illustrated in Fig. 4. It may be observed that the CNN-LSTM model has better performance than CNN only model in x and y directions. The LSTM layer utilized in the model is able to learn temporal features of the pre-movement EEG data utilized as the input. Transient movement in z-direction adds to the uncertainty of the model.

3D hand trajectory decoding using different EEG window sizes is investigated in Section 4.1.4. The pre-movement EEG data, with at-least 50 ms prior to the movement-onset, has been utilized for hand trajectory decoding. Best correlation is achieved for −350 ms to −50 ms window (refer to Table 4). Reasonable accuracy is achieved even for −350 ms to −100 ms window. This shows the feasibility to decode hand trajectory using pre-movement scalp EEG signals. The results are in line with the fact that the motor movement is encoded in EEG signal around 300 ms prior to the movement [43]. Trajectory estimation using pre-movement EEG data will be helpful in BCI applications such as controlling prosthesis and human power-augmentation exosuit.

The performance of the proposed movement decoders is analyzed for inter-subject variability. Such EEG-based inter-subject study is sparse in the literature. One of the reasons for the same is low-performance capability. The low performance is due to the inability of the model to learn the appropriate features across subjects. Jeong et al. reported a grand average correlation value of 0.08 for the multi-direction arm reaching task in the three axes using the CNN-BiLSTM neural network [41]. The proposed CNN-LSTM model for trajectory decoding during the grasp and lift task has decent decoding performance with a grand mean PCC of 0.627 with a 350 ms EEG window (refer to Table 5).

6. Conclusions and future work

In this study, deep learning based neural decoders have been proposed for efficient 3D hand kinematics decoding using pre-movement EEG signals. In particular, MLP and CNN-LSTM based models are proposed. The pre-movement neural information encoded in EEG signals has been utilized for efficient hand trajectory decoding. Frequency band analysis for 3D hand kinematics decoding have been investigated. Various EEG lag windows have been utilized for trajectory intention detection. Additionally, the feasibility of inter-subject hand trajectory decoding has been examined. PCC analysis is utilized to establish the effectiveness of proposed neural decoders. Continuous trajectory estimation using EEG signals has potential application in real-time BCI for healthy subjects and amputees. The application includes neuro-rehabilitation, neuro-prosthetics, and neural-driven exosuits. Subject-independent BCI systems for real-time control of BCI system remains an open problem.

CRediT authorship contribution statement

Anant Jain: Conceptualization, Methodology, Software, Validation, Formal analysis, Writing – original draft. **Lalan Kumar:** Conceptualization, Methodology, Supervision, Formal analysis, Writing – review & editing.

Declaration of competing interest

The authors declare that they have no known competing financial interests or personal relationships that could have appeared to influence the work reported in this paper.

Data availability

Open access dataset (WAY-EEG-GAL) was utilized in this study.

Acknowledgments

This research work was supported in part by DRDO - JATC project with project number RP04191G. The authors would like to thank Prof. Sitikantha Roy and Prof. Shubhendu Bhasin from Indian Institute of Technology Delhi (IITD), and Dr. Suriya Prakash from All India Institute of Medical Sciences (AIIMS) Delhi for their discussion and constructive comments during the preparation of the manuscript.

Table 5
Inter-Subject analysis of neural decoders ((a) mLR, (b) MLP, and (c) CNN-LSTM) with window size of 150 ms, 200 ms, 250 ms, 300 ms and 350 ms.

EEG window	Decoders	Direction	SUBJECT AS TEST_DATA (LEAVE ONE SUBJECT OUT)												
			S01	S02	S03	S04	S05	S06	S07	S08	S09	S10	S11	S12	Average
−150 to 0	(a)	x	0.431	0.177	0.296	0.401	0.297	0.305	0.248	0.178	0.312	0.389	0.153	0.123	0.123
		y	0.434	0.181	0.300	0.413	0.284	0.289	0.246	0.178	0.314	0.399	0.159	0.144	0.144
		z	0.309	0.115	0.306	0.334	0.293	0.138	0.257	0.254	0.199	0.224	0.179	0.287	0.287
	(b)	x	0.681	0.684	0.685	0.735	0.774	0.779	0.743	0.764	0.768	0.779	0.687	0.651	0.651
		y	0.719	0.697	0.705	0.748	0.793	0.795	0.755	0.768	0.787	0.785	0.709	0.688	0.688
		z	0.586	0.359	0.702	0.644	0.604	0.526	0.428	0.666	0.461	0.635	0.362	0.429	0.429
	(c)	x	0.655	0.703	0.707	0.731	0.775	0.788	0.752	0.767	0.762	0.791	0.696	0.635	0.635
		y	0.697	0.713	0.727	0.738	0.789	0.802	0.761	0.773	0.783	0.795	0.716	0.671	0.671
		z	0.536	0.335	0.667	0.592	0.538	0.507	0.400	0.632	0.440	0.594	0.345	0.405	0.405
−200 to 0	(a)	x	0.423	0.211	0.288	0.364	0.301	0.275	0.267	0.170	0.325	0.136	0.099	0.106	0.106
		y	0.415	0.213	0.295	0.379	0.291	0.260	0.261	0.171	0.327	0.123	0.106	0.120	0.120
		z	0.307	0.198	0.269	0.349	0.289	0.151	0.274	0.235	0.212	0.210	0.186	0.302	0.302
	(b)	x	0.669	0.692	0.720	0.723	0.779	0.804	0.755	0.765	0.789	0.745	0.660	0.655	0.655
		y	0.708	0.701	0.742	0.733	0.798	0.817	0.765	0.775	0.813	0.750	0.695	0.697	0.697
		z	0.575	0.412	0.711	0.645	0.591	0.549	0.432	0.674	0.483	0.603	0.373	0.465	0.465
	(c)	x	0.680	0.722	0.723	0.736	0.790	0.801	0.758	0.786	0.778	0.769	0.672	0.657	0.657
		y	0.720	0.735	0.741	0.750	0.808	0.818	0.767	0.796	0.802	0.776	0.699	0.693	0.693
		z	0.532	0.385	0.656	0.586	0.561	0.512	0.396	0.633	0.441	0.554	0.331	0.439	0.439
−250 to 0	(a)	x	0.418	0.170	0.289	0.360	0.286	0.261	0.262	0.143	0.305	0.099	0.072	0.100	0.100
		y	0.406	0.175	0.293	0.374	0.281	0.243	0.246	0.143	0.308	0.084	0.078	0.106	0.106
		z	0.295	0.217	0.255	0.356	0.266	0.159	0.286	0.224	0.232	0.187	0.143	0.318	0.318
	(b)	x	0.677	0.697	0.712	0.744	0.761	0.794	0.764	0.777	0.771	0.750	0.693	0.644	0.644
		y	0.714	0.711	0.734	0.754	0.788	0.805	0.775	0.782	0.796	0.761	0.715	0.690	0.690
		z	0.599	0.405	0.712	0.661	0.609	0.547	0.451	0.674	0.486	0.627	0.349	0.484	0.484
	(c)	x	0.669	0.716	0.712	0.748	0.793	0.801	0.768	0.789	0.764	0.773	0.676	0.684	0.684
		y	0.705	0.724	0.729	0.759	0.812	0.813	0.779	0.797	0.785	0.780	0.703	0.722	0.722
		z	0.551	0.385	0.665	0.570	0.538	0.482	0.403	0.632	0.443	0.545	0.298	0.455	0.455
−300 to 0	(a)	x	0.439	0.133	0.262	0.357	0.270	0.346	0.235	0.134	0.275	0.132	0.069	0.091	0.091
		y	0.431	0.141	0.265	0.380	0.270	0.340	0.218	0.130	0.276	0.121	0.073	0.094	0.094
		z	0.272	0.135	0.211	0.341	0.226	0.171	0.272	0.224	0.250	0.196	0.171	0.317	0.317
	(b)	x	0.692	0.679	0.705	0.728	0.763	0.822	0.759	0.765	0.769	0.755	0.660	0.635	0.635
		y	0.728	0.697	0.728	0.738	0.788	0.835	0.770	0.774	0.785	0.766	0.682	0.683	0.683
		z	0.620	0.368	0.710	0.642	0.576	0.592	0.452	0.687	0.499	0.618	0.369	0.478	0.478
	(c)	x	0.708	0.713	0.730	0.734	0.798	0.800	0.776	0.787	0.772	0.779	0.697	0.655	0.655
		y	0.743	0.733	0.749	0.745	0.820	0.819	0.791	0.798	0.795	0.788	0.719	0.694	0.694
		z	0.574	0.325	0.628	0.532	0.498	0.513	0.397	0.607	0.430	0.525	0.307	0.414	0.414
−350 to 0	(a)	x	0.463	0.143	0.301	0.339	0.272	0.258	0.248	0.137	0.265	0.134	0.076	0.080	0.080
		y	0.452	0.155	0.299	0.363	0.273	0.244	0.228	0.136	0.264	0.119	0.075	0.079	0.079
		z	0.248	0.160	0.205	0.343	0.207	0.177	0.260	0.200	0.264	0.167	0.149	0.317	0.317
	(b)	x	0.686	0.707	0.713	0.716	0.775	0.806	0.754	0.759	0.765	0.767	0.692	0.631	0.631
		y	0.728	0.725	0.729	0.727	0.800	0.812	0.765	0.767	0.788	0.776	0.710	0.673	0.673
		z	0.611	0.400	0.700	0.636	0.591	0.569	0.459	0.676	0.497	0.617	0.378	0.495	**0.495**
	(c)	x	0.728	0.726	0.737	0.747	0.808	0.810	0.787	0.799	0.776	0.798	0.712	0.690	**0.690**
		y	0.764	0.746	0.753	0.753	0.829	0.829	0.790	0.805	0.799	0.807	0.732	0.728	**0.728**
		z	0.565	0.365	0.620	0.498	0.487	0.506	0.385	0.617	0.434	0.519	0.313	0.462	0.462

Note: the bold entries represent the highest mean PCC value obtained using the neural decoders in x, y and z directions.

References

[1] A. Kübler, The history of BCI: From a vision for the future to real support for personhood in people with locked-in syndrome, Neuroethics 13 (2) (2020) 163–180.

[2] U. Chaudhary, N. Birbaumer, A. Ramos-Murguialday, Brain-computer interfaces for communication and rehabilitation, Nat. Rev. Neurol. 12 (9) (2016) 513–525.

[3] M. Coscia, M.J. Wessel, U. Chaudary, J.d.R. Millán, S. Micera, A. Guggisberg, P. Vuadens, J. Donoghue, N. Birbaumer, F.C. Hummel, Neurotechnology-aided interventions for upper limb motor rehabilitation in severe chronic stroke, Brain 142 (8) (2019) 2182–2197.

[4] B. Hobbs, P. Artemiadis, A review of robot-assisted lower-limb stroke therapy: Unexplored paths and future directions in gait rehabilitation, Front. Neurorobotics 14 (2020) 19.

[5] M.L. Chen, D. Fu, J. Boger, N. Jiang, Age-related changes in vibro-tactile EEG response and its implications in BCI applications: A comparison between older and younger populations, IEEE Trans. Neural Syst. Rehabil. Eng. 27 (4) (2019) 603–610.

[6] J. Jin, Z. Chen, R. Xu, Y. Miao, X. Wang, T.-P. Jung, Developing a novel tactile P300 brain-computer interface with a cheeks-stim paradigm, IEEE Trans. Biomed. Eng. 67 (9) (2020) 2585–2593.
[7] N. Robinson, R. Mane, T. Chouhan, C. Guan, Emerging trends in BCI-robotics for motor control and rehabilitation, Curr. Opin. Biomed. Eng. 20 (2021) 100354.
[8] S. Waldert, Invasive vs. non-invasive neuronal signals for brain-machine interfaces: Will one prevail? Front. Neurosci. 10 (2016) 295.
[9] S.J. Jang, Y.J. Yang, S. Ryun, J.S. Kim, C.K. Chung, J. Jeong, Decoding trajectories of imagined hand movement using electrocorticograms for brain–machine interface, J. Neural Eng. 19 (5) (2022) 056011.
[10] J. Mellinger, G. Schalk, C. Braun, H. Preissl, W. Rosenstiel, N. Birbaumer, A. Kübler, An MEG-based Brain–Computer Interface (BCI), Neuroimage 36 (3) (2007) 581–593.
[11] R. Alazrai, H. Alwanni, M.I. Daoud, EEG-based BCI system for decoding finger movements within the same hand, Neurosci. Lett. 698 (2019) 113–120.
[12] S. Hosni, S. Borgheai, J. McLinden, Y. Shahriari, An fNIRS-based motor imagery BCI for ALS: A subject-specific data-driven approach, IEEE Trans. Neural Syst. Rehabil. Eng. 28 (12) (2020) 3063–3073.
[13] Z. Liu, J. Shore, M. Wang, F. Yuan, A. Buss, X. Zhao, A systematic review on hybrid EEG/fNIRS in brain-computer interface, Biomed. Signal Process. Control 68 (2021) 102595.
[14] H.I. Baqapuri, L.D. Roes, M. Zvyagintsev, S. Ramadan, M. Keller, E. Roecher, J. Zweerings, M. Klasen, R.C. Gur, K. Mathiak, A novel brain-computer interface virtual environment for neurofeedback during functional MRI, Front. Neurosci. 14 (2021) 593854.
[15] A. Kline, N.D. Forkert, B. Felfeliyan, D. Pittman, B. Goodyear, J. Ronsky, fMRI-Informed EEG for brain mapping of imagined lower limb movement: Feasibility of a brain computer interface, J. Neurosci. Methods 363 (2021) 109339.
[16] D. McFarland, J. Wolpaw, EEG-based brain–computer interfaces, Curr. Opin. Biomed. Eng. 4 (2017) 194–200.
[17] D. Maheshwari, S.K. Ghosh, R. Tripathy, M. Sharma, U.R. Acharya, Automated accurate emotion recognition system using rhythm-specific deep convolutional neural network technique with multi-channel EEG signals, Comput. Biol. Med. 134 (2021) 104428.
[18] J. Li, H. Hua, Z. Xu, L. Shu, X. Xu, F. Kuang, S. Wu, Cross-subject EEG emotion recognition combined with connectivity features and meta-transfer learning, Comput. Biol. Med. 145 (2022) 105519.
[19] M. Barsotti, D. Leonardis, C. Loconsole, M. Solazzi, E. Sotgiu, C. Procopio, C. Chisari, M. Bergamasco, A. Frisoli, A full upper limb robotic exoskeleton for reaching and grasping rehabilitation triggered by MI-BCI, in: 2015 IEEE International Conference on Rehabilitation Robotics, ICORR, IEEE, 2015, pp. 49–54.
[20] G. Yu, J. Wang, W. Chen, J. Zhang, EEG-based brain-controlled lower extremity exoskeleton rehabilitation robot, in: 2017 IEEE International Conference on Cybernetics and Intelligent Systems (CIS) and IEEE Conference on Robotics, Automation and Mechatronics, RAM, IEEE, 2017, pp. 763–767.
[21] M. Tariq, P.M. Trivailo, M. Simic, EEG-based BCI control schemes for lower-limb assistive-robots, Front. Hum. Neurosci. 12 (2018) 312.
[22] M.S. Al-Quraishi, I. Elamvazuthi, S.A. Daud, S. Parasuraman, A. Borboni, EEG-based control for upper and lower limb exoskeletons and prostheses: A systematic review, Sensors 18 (10) (2018) 3342.
[23] Q. Huang, Z. Zhang, T. Yu, S. He, Y. Li, An EEG-/EOG-based hybrid brain-computer interface: Application on controlling an integrated wheelchair robotic arm system, Front. Neurosci. 13 (2019) 1243.
[24] H. Gao, L. Luo, M. Pi, Z. Li, Q. Li, K. Zhao, J. Huang, EEG-based volitional control of prosthetic legs for walking in different terrains, IEEE Trans. Autom. Sci. Eng. 18 (2) (2019) 530–540.
[25] Y. Zhu, Y. Li, J. Lu, P. Li, A hybrid BCI based on SSVEP and EOG for robotic arm control, Front. Neurorobotics 14 (2020) 583641.
[26] M. Nann, F. Cordella, E. Trigili, C. Lauretti, M. Bravi, S. Miccinilli, J.M. Catalan, F.J. Badesa, S. Crea, F. Bressi, et al., Restoring activities of daily living using an EEG/EOG-controlled semiautonomous and mobile whole-arm exoskeleton in chronic stroke, IEEE Syst. J. 15 (2) (2020) 2314–2321.
[27] L. Cao, G. Li, Y. Xu, H. Zhang, X. Shu, D. Zhang, A brain-actuated robotic arm system using non-invasive hybrid brain-computer interface and shared control strategy, J. Neural Eng. 18 (4) (2021) 046045.
[28] Y. Mishchenko, M. Kaya, E. Ozbay, H. Yanar, Developing a three-to six-state EEG-based brain–computer interface for a virtual robotic manipulator control, IEEE Trans. Biomed. Eng. 66 (4) (2018) 977–987.
[29] B.J. Edelman, B. Baxter, B. He, EEG source imaging enhances the decoding of complex right-hand motor imagery tasks, IEEE Trans. Biomed. Eng. 63 (1) (2015) 4–14.
[30] P. Ofner, A. Schwarz, J. Pereira, G.R. Müller-Putz, Upper limb movements can be decoded from the time-domain of low-frequency EEG, PLoS One 12 (8) (2017) e0182578.
[31] G. Liu, L. Tian, W. Zhou, Multiscale time-frequency method for multiclass motor imagery brain computer interface, Comput. Biol. Med. 143 (2022) 105299.
[32] P. Rithwik, V. Benzy, A. Vinod, High accuracy decoding of motor imagery directions from EEG-based brain computer interface using filter bank spatially regularised common spatial pattern method, Biomed. Signal Process. Control 72 (2022) 103241.
[33] R. Chaisaen, P. Autthasan, N. Mingchinda, P. Leelaarporn, N. Kunaseth, S. Tammajarung, P. Manoonpong, S.C. Mukhopadhyay, T. Wilaiprasitporn, Decoding EEG rhythms during action observation, motor imagery, and execution for standing and sitting, IEEE Sens. J. 20 (22) (2020) 13776–13786.
[34] O. Özdenizci, S.Y. Günay, F. Quivira, D. Erdoğmuş, Hierarchical graphical models for context-aware hybrid brain-machine interfaces, in: 2018 40th Annual International Conference of the IEEE Engineering in Medicine and Biology Society, EMBC, IEEE, 2018, pp. 1964–1967.
[35] A. Schwarz, J. Pereira, R. Kobler, G.R. Müller-Putz, Unimanual and bimanual reach-and-grasp actions can be decoded from human EEG, IEEE Trans. Biomed. Eng. 67 (6) (2019) 1684–1695.
[36] J.-H. Cho, J.-H. Jeong, S.-W. Lee, Neurograsp: Real-time EEG classification of high-level motor imagery tasks using a dual-stage deep learning framework, IEEE Trans. Cybern. (2021).
[37] J.-H. Cho, B.-H. Kwon, B.-H. Lee, S.-W. Lee, Decoding continual muscle movements related to complex hand grasping from EEG signals, in: 2022 10th International Winter Conference on Brain-Computer Interface, BCI, IEEE, 2022, pp. 1–5.
[38] N. Robinson, C. Guan, A. Vinod, Adaptive estimation of hand movement trajectory in an EEG based brain-computer interface system, J. Neural Eng. 12 (6) (2015) 066019.
[39] A. Korik, R. Sosnik, N. Siddique, D. Coyle, Decoding imagined 3D hand movement trajectories from EEG: Evidence to support the use of mu, beta, and low gamma oscillations, Front. Neurosci. 12 (2018) 130.
[40] R. Sosnik, O.B. Zur, Reconstruction of hand, elbow and shoulder actual and imagined trajectories in 3D space using EEG slow cortical potentials, J. Neural Eng. 17 (1) (2020) 016065.
[41] J.-H. Jeong, K.-H. Shim, D.-J. Kim, S.-W. Lee, Brain-controlled robotic arm system based on multi-directional CNN-BiLSTM network using EEG signals, IEEE Trans. Neural Syst. Rehabil. Eng. 28 (5) (2020) 1226–1238.
[42] J. Fernández-Vargas, T.V. Tarvainen, K. Kita, W. Yu, Effects of using virtual reality and virtual avatar on hand motion reconstruction accuracy and brain activity, IEEE Access 5 (2017) 23736–23750.
[43] S. Pancholi, A. Giri, A. Jain, L. Kumar, S. Roy, Source aware deep learning framework for hand kinematic reconstruction using EEG signal, IEEE Trans. Cybern. (2022) 1–13, http://dx.doi.org/10.1109/TCYB.2022.3166604.
[44] A. Jain, L. Kumar, PreMovNet: Premovement EEG-based hand kinematics estimation for grasp-and-lift task, IEEE Sensors Lett. 6 (7) (2022) 1–4, http://dx.doi.org/10.1109/LSENS.2022.3183284.
[45] M.D. Luciw, E. Jarocka, B.B. Edin, Multi-channel EEG recordings during 3,936 grasp and lift trials with varying weight and friction, Sci. Data 1 (1) (2014) 1–11.
[46] A. Delorme, S. Makeig, EEGLAB: An open source toolbox for analysis of single-trial EEG dynamics including independent component analysis, J. Neurosci. Methods 134 (1) (2004) 9–21.
[47] D.P. Kingma, J. Ba, Adam: A method for stochastic optimization, 2014, arXiv preprint arXiv:1412.6980.
[48] T. Chouhan, N. Robinson, A. Vinod, K.K. Ang, C. Guan, Wavlet phase-locking based binary classification of hand movement directions from EEG, J. Neural Eng. 15 (6) (2018) 066008.
[49] S.M. Hosseini, V. Shalchyan, Continuous decoding of hand movement from EEG signals using phase-based connectivity features, Front. Hum. Neurosci. (2022) 408.